Sensors and Actuators A 321 (2021) 112598

Contents lists available at ScienceDirect

Sensors and Actuators A: Physical

journal homepage: www.elsevier.com/locate/sna

Shape memory alloy based 3D printed composite actuators with variable stiffness and large reversible deformation

Saeed Akbari [a,*,1], Amir Hosein Sakhaei [b,1], Sahil Panjwani [c,1], Kavin Kowsari [c], Qi Ge [c,d,**]

[a] RISE Research Institutes of Sweden, Box 104, SE-431 22, Mölndal, Sweden
[b] School of Engineering and Digital Arts, University of Kent, Canterbury, CT2 7NT, UK
[c] Digital Manufacturing and Design Center, Singapore University of Technology and Design, 487372, Singapore
[d] Department of Mechanical and Energy Engineering, Southern University of Science and Technology, 518055, China

ARTICLE INFO

Article history:
Received 27 July 2020
Received in revised form 28 January 2021
Accepted 29 January 2021
Available online 2 February 2021

Keywords:
3D printing
Composite actuator
Shape memory alloy
Shape memory polymer
Finite element modeling

ABSTRACT

Soft composite actuators can be fabricated by embedding shape memory alloy (SMA) wires into soft polymer matrices. Shape retention and recovery of these actuators are typically achieved by incorporating shape memory polymer segments into the actuator structure. However, this requires complex manufacturing processes. This work uses multimaterial 3D printing to fabricate composite actuators with variable stiffness capable of shape retention and recovery. The hinges of the bending actuators presented here are printed from a soft elastomeric layer as well as a rigid shape memory polymer (SMP) layer. The SMA wires are embedded eccentrically over the entire length of the printed structure to provide the actuation bending force, while the resistive wires are embedded into the SMP layer of the hinges to change the temperature and the bending stiffness of the actuator hinges via Joule heating. The temperature of the embedded SMA wire and the printed SMP segments is changed sequentially to accomplish a large bending deformation, retention of the deformed shape, and recovery of the original shape, without applying any external mechanical force. The SMP layer thickness was varied to investigate its effect on shape retention and recovery. A nonlinear finite element model was used to predict the deformation of the actuators.

1. Introduction

Shape memory alloys (SMAs) can be trained under a combination of thermal and mechanical loads to take a temporary elongated shape, and then contract to recover their original shape. This results from transformations between a martensite phase at low temperatures and an austenite phase at high temperature. Over the past three decades, this class of active materials has been widely used in fabricating various shape memory structures and actuators [1–7].

However, the recoverable strain of the SMAs is only 4–8%, which limits their maximum achievable stroke [8]. An alternative approach is to integrate the small deformation of the SMA wires into a polymer soft matrix to produce diverse types of large deformations such as bending, twisting, and coupled bending-twisting. A common method to produce bending motions using this approach is to embed the SMA wires at an eccentric distance from the neutral axis of an elastic beam with a low bending stiffness. Upon actuation, axial contraction of the SMA wire is converted into a large bending deformation [9–11].

The bodies of SMA based soft actuators are conventionally fabricated in custom designed moulds with multiple assembly steps [9,10,12–17], which are performed manually and may lead to inconsistent fabrication repeatability. Moreover, these actuators are limited by their inability to remain stable in the actuated shape. Actuator shape retention can be achieved by maintaining the SMA wire in the actuated state. However, continuous actuation of the SMA wire for a long time increases the required energy. Several research works have tried to address this issue by incorporating phase changeable materials such as fusible alloys [11,18] and polymers [19,20] into the actuator. These materials exhibit temperature dependent stiffness, and are incorporated into the actuator as substructures to enable stiffness modulation. If a phase changeable material with shape recovery capability such as SMP is used, the actuator can also demonstrate reversible deformation [17,19,21]. However, accurate placement of these additional substructures within the actuator presents practical challenges, and increases the cost and time of manufacturing.

* Corresponding author.
** Corresponding author at: Department of Mechanical and Energy Engineering, Southern University of Science and Technology, 518055, China.
E-mail addresses: saeed.akbari@ri.se (S. Akbari), geq@sustech.edu.cn (Q. Ge).
[1] These authors contributed equally to this work.

https://doi.org/10.1016/j.sna.2021.112598

These issues necessitate a more flexible fabrication technology that obviates the need for complex molding and assembly techniques required in the conventional manufacturing methods. The fabrication method should be able to facilitate the implementation of proper actuator design principles, including tunable mechanical properties and morphological complexity. This study proposes multimaterial inkjet 3D printing as an alternative approach to fabricate SMA based composite actuators with variable stiffness that are capable of shape retention and shape recovery. This technology is able to deposit various digital materials with a broad range of properties in micron scale [22–25]. It enables customized design of the actuator based on the structural and performance requirements such as bending stiffness and recovery ratio. It also enables rapid design modification and iteration with no additional cost.

In a former study [26], we demonstrated SMA-based soft actuators whose matrix was printed from an elastomer. Those actuators were not capable of shape retention and recovery. To extend that study, in this work, SMA-SMP composite actuators with variable stiffness are fabricated using multimaterial inkjet 3D printing. The actuators consist of two hinges, printed from rigid SMP segments and an elastomeric soft layer. The stiffness modulation for shape retention and recovery is achieved using embedded SMP segments of different thicknesses, whose temperature in the hinge area is controlled through Joule heating to transform them from a high stiffness state at room temperature to a low stiffness state at elevated temperatures. When the SMP is at the low stiffness state, actuation of the SMA wire results in a large bending deformation in the hinge area. The shape memory of the SMPs also enables the recovery of the original shape at high temperatures. The performance of the actuator, including bending stiffness and maximum deformation, is measured for a variety of actuators to show versatility of multimaterial 3D printing. A finite element model is also developed to determine important actuation parameters including shape fixity and recovery. It incorporates user material subroutines (UMATs) to model nonlinear temperature dependant behaviour of the SMA and the SMP.

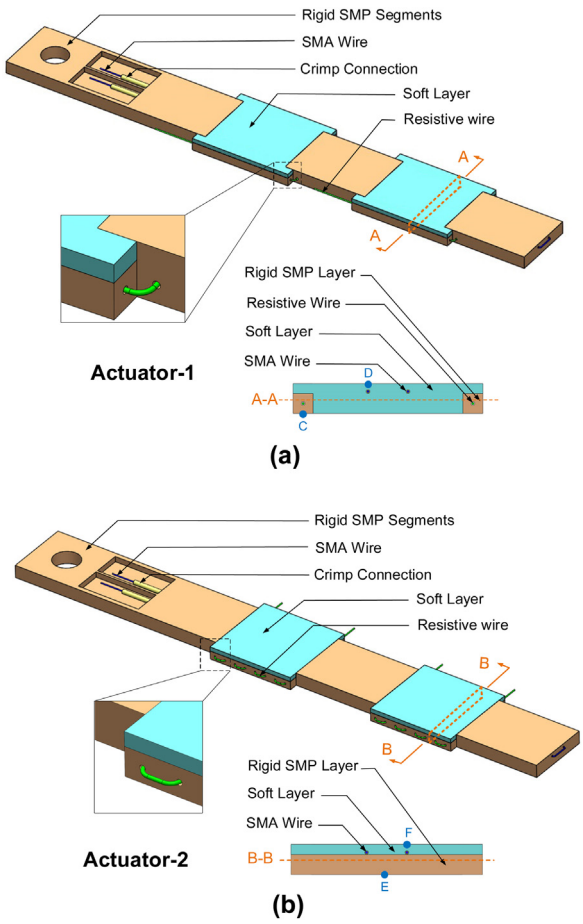

Fig. 1. Two basic designs of the composite actuators with two hinges. The SMA wire is inserted into the actuator over the entire length, while resistive wires are inserted in to the SMP segments of each hinge. a) Actuator-1 with resistive wires embedded in the SMP segments printed longitudinally on both sides of each hinge. b) Actuator-2 with resistive wires embedded transversely into the SMP layer at the bottom of each hinge.

2. Materials and methods

2.1. Design of actuators

The printed actuators are capable of large bending deformations in a low-stiffness state, retaining the deformed shape in a high-stiffness state, and then recovering the original as-fabricated shape in a low-stiffness state. In order to demonstrate the flexibility of multimaterial 3D printing, two basic designs are used for the bending actuators, as shown in Fig. 1. Each actuator has a thickness of 3 mm, a width of 15 mm, and an effective length of 100 mm, with two 20 mm long hinges. Each hinge has embedded SMP segments whose temperature is controlled via Joule heating. Resistive wires are embedded into the designated holes in the hinge areas to effectively control the temperature of the SMP segments, which serve two functions: shape retention of the deformed actuator at temperatures lower than the glass transition temperature ($T<T_g$), and shape recovery at elevated temperatures ($T>T_g$).

The first design, introduced in Fig. 1a and referred to as Actuator-1 hereafter, is comprised of two slender rectangular SMP bars which are printed on each side of the actuator in parallel to the SMA wires. However, in the second design, referred to as Actuator-2, the SMP segment is printed in the form of a thin layer on the bottom of each hinge. As shown in Cross-Section A-A of Actuator-1 (Fig. 1a), and Cross-Section B-B of Actuator-2 (Fig. 1b), the volume fraction of the soft material within the hinges of Actuator-1 is significantly higher than Actuator-2. Therefore, the two actuators have different bending stiffnesses in the hinge area. The original thickness of the SMP segments was 2 mm but was changed in a number of experiments and simulations to investigate its effect on the fixity and recovery ratios of the actuators. The performance difference between the two designs is studied in detail in the following sections.

In both bending designs, the SMA wire is first prestrained by 5%, and then embedded eccentrically to the printed composite structure. Once actuated via Joule heating, it is contracted to restore its initial shape, thus applies a compression force to the actuator at an off-axis distance with respect to its midplane, which results in bending deformation in the hinge area, and deforms it when it is in the low stiffness state at high temperatures. As shown in Fig. 1, the temperature of the SMP segments of each hinge is separately controlled by the inserted resistive wires to deform each hinge independently.

Fig. 2 shows the timing sequence of the actuation of the resistive and SMA wires. First, the SMP sub-structures in the hinge area are heated using resistive wires by applying the current I_1 from the beginning to the time t_1 to transform them from a glassy (high-stiffness) state to a rubbery (low-stiffness) state. Then, the input current to the resistive wire is stopped, and the SMA wire is actuated by applying I_2 from t_1 to t_2 to produce a large bending deformation. The SMA wire remains actuated until the SMP cools down to the high-stiffness glassy state. After the SMA wire is deactivated, the actuator retains the deformed shape due to the high-stiffness of the SMP sub-structures. Finally, applying current I_1 again to the resistive wire increases the temperature of the SMP,

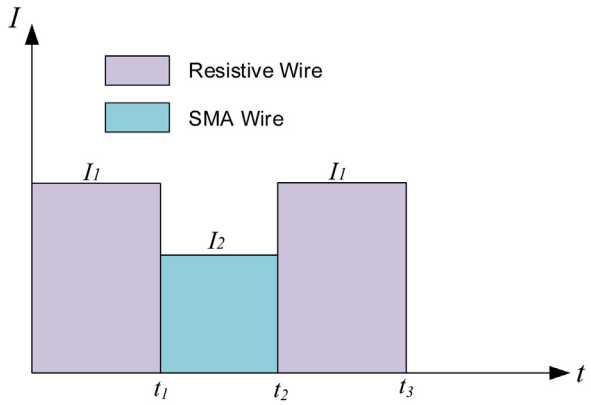

Fig. 2. The current is applied to the resistive and SMA wires sequentially to realize deformation, shape retention, and shape recovery.

and results in shape recovery of the actuator. The required electrical current to actuate the resistive and SMA wires was extensively explored during experimentation to determine effective testing conditions for actuator designs introduced in Fig. 1.

2.2. Experimental procedure

A multimaterial inkjet 3D printer (Objet500 Connex 3, Stratasys, Edina, MN, USA) was used to print the body of the composite actuators. This printer is able to print two base polymer materials, including a soft elastomeric polymer, known as Agilus30, and a rigid polymer, known as VeroClear. It is also able to print various combinations of these two base materials on a voxelized domain to create digital materials with a broad range of properties between the two base materials.

Characterization of mechanical properties of printed materials facilitates the design of the composite actuators. For this purpose, a series of uniaxial tensile tests and dynamic mechanical analysis (DMA) tests were conducted. Fig. 3a and b show the change with temperature of stress-strain behaviour, failure strain and Young's modulus of VeroClear, which was selected to print the SMP substructures owing to its highly temperature-dependent stiffness, which enables the shape retention capability. The failure strain was assumed to be the strain at the moment of sample rupture (the maximum recorded strain). Young's modulus of VeroClear changes from 1387 MPa at room temperature to 16 MPa at 60 °C. In addition, VeroClear has excellent shape memory behaviour as demonstrated in previous studies [22–25], which allows for recovery of the original shape of the actuator.

Fig. 3c and d illustrate the tensile properties of the elastomeric digital materials measured at room temperature. From Agilus30 to FLX9950, Young's modulus increases while the failure strain decreases. Among the tested digital materials, FLX9960 (E = 2.6 MPa) was selected to print the actuator soft segments, because its stiffness is very close to polydimethylsiloxane (PDMS, E = 1.8 MPa), an elastomer widely used in the conventional fabrication methods of soft actuators [9,10,14].

The results of the DMA tests are shown in Fig. 4. The T_g of the printed materials was recognized as a peak in the Tanδ curve in Fig. 4a, and plotted in Fig. 4b. According to the DMA tests, the T_g of VeroClear and FLX9960 is 58 °C and 4 °C, respectively. At temperatures higher than T_g, VeroClear is in a rubbery state.

Bending actuators including Actuator-1 and Actuator-2 (Fig. 1) were printed using the multimaterial inkjet printer. After printing, the residual support material from the 3D printed parts was cleared using a high pressure water cleaner (Powerblast, Balco Engineering Ltd, Birmingham, UK). After removing all of the support material, the SMA wire, which was a nickel-titanium alloy (Flexinol, Irvine, CA, USA, properties of Table 1) with a diameter of 0.15 mm, was embedded into the printed composite structure and fixed to the two designated points at one end of the actuator using copper crimp connections (Insulated Crimp Bootlace Ferrule, RS Components, Corby, UK) to prevent relative sliding between the soft matrix and the SMA wire.

In addition, the resistive wire was selected from a copper–nickel alloy, referred to as Constantan (Block Transformatoren-Elektronik

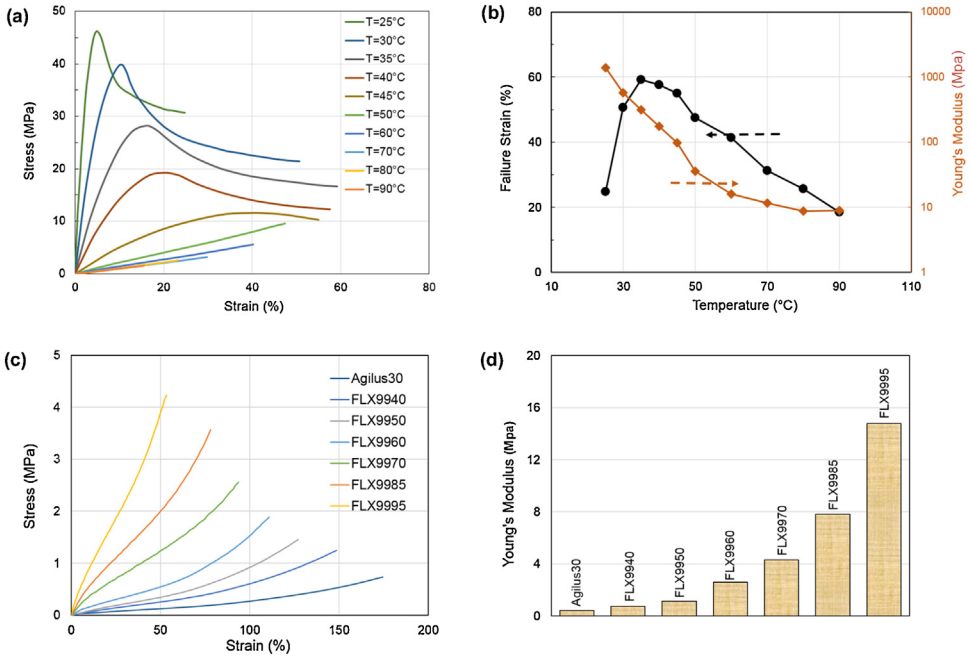

Fig. 3. Results of the uniaxial tensile tests of the printed materials. a) Stress-strain behavior of VeroClear at different temperatures, which was used to print the SMP segments of the actuators. b) Failure strain and Young's modulus of VeroClear versus temperature. c) Stress-strain behavior of the elastomeric digital materials at room temperature, which were used to print the soft segments of the actuators. d) Young's modulus of the elastomeric digital materials at room temperature.

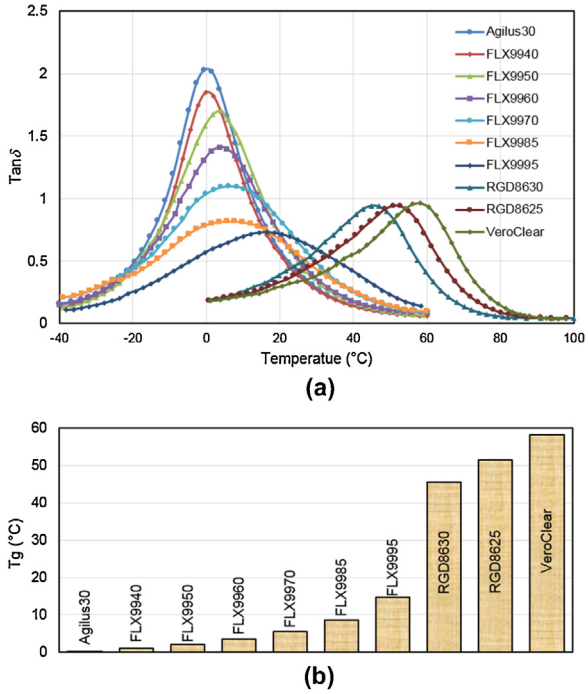

Fig. 4. Results of DMA tests for various printed materials. a) Tanδ vs temperature. b) T_g of the printed materials.

GmbH, Verden, Germany), with a thickness of 0.20 mm and a resistance of 15.6 Ω/m, and inserted into the SMP segments in the hinge area. A programmable power supply (HMP4030, Rohde & Schwarz, Munich, Germany) was used to apply the designated current to each wire for a predetermined amount of time.

3. Finite element modelling

The three-dimensional finite element simulations were conducted in the software ABAQUS to analyze the thermo-mechanical behaviour of the printed actuators based on the experimental conditions. The goal of the analysis was to present and validate a computational framework which could be used for further development of actuators capable of complex deformations. Fig. 5 illustrates the 3D finite element model of Actuator-1 with prescribed displacement-based boundary conditions at one end.

Three different material models were used to simulate the soft layer, the SMP, and the SMA. Regarding the material characterization results (Fig. 3), the soft layer was assumed to have linear elastic behavior. For the SMA wire, a coupled thermo-mechanical, isotropic-based material model was used. It was developed and implemented as an ABAQUS user-defined material (UMAT) in [27,28]. Furthermore, another UMAT was used for the SMP, which was developed based on a multi-branch viscoelastic constitutive model comprehensively explained in [29,30].

The SMP segments of the actuator were modelled using 3568 continuum linear hexahedral elements of type C3D8H, and the SMA was modelled using 109 continuum linear line elements of type B31H. Furthermore, a surface-to-surface frictionless contact was

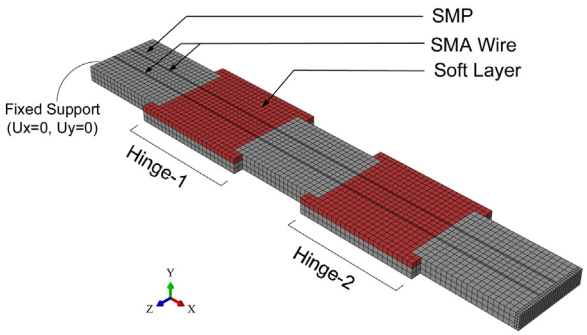

Fig. 5. 3D finite element model of Actuator-1 (Fig. 1a). Two separate UMATs were used to model nonlinear large deformation of the SMP and SMA.

assumed at the interface between the SMA wire and the inner wall of the hole embedded in the longitudinal direction of the actuator.

The loading steps for the model are as follows. First, the SMA wire is extended 5% at room temperature when the material is in the martensitic phase. Second, the SMA wire is unloaded when it is still at the room temperature. These two steps cause 5% strain in the SMA wire due to the detwinning in the martensitic phase.

As shown in Fig. 1, the temperature of the SMP segment in each hinge area is independently controlled using the embedded resistive wires. In the next step of simulation, the temperature of the SMP segment in the desired hinge is increased to over T_g. As a result, the SMP in the hinge becomes soft. It should be noted that the heating does not affect the other SMP segments, and they remain rigid at room temperature. In the next step, the contact between the SMA wire and the matrix is activated, and the SMA temperature is increased to a temperature higher than the austenitic finish temperature (A_s = 78 °C, Table 1). This leads to the recovery of 5% strain stored in the wire, and bending deformation of the actuator due to the wire contraction. Then, the temperature of the hinge SMP is decreased. This transforms the SMP layer to the stiffer glassy state. In the next step, the SMA wire is deactivated by reducing its temperature to room temperature. After this step, the deformed shape of the actuator is retained owing to the rigidity of the SMP segment of the hinge. Finally, the hinge SMP is heated up again to restore the actuator original shape. These steps are demonstrated in greater detail and compared with the experimental results in the next section.

4. Results and discussion

By 3D printing several test specimens, the performance of Actuator-1 and Actuator-2 (Fig. 1) was experimentally measured. First, a series of measurements were conducted to investigate the effect of applied current on the heating time and bending stiffness of the SMP segments. Temperature of the SMP segments was measured using an infrared thermometer camera (Fluke 297 FC, Fluke Co., Everett, WS, USA). The actuator temperature near the SMP segments was measured on Point C for Actuator-1 (Fig. 1a) and Point E for Actuator-2 (Fig. 1b). Fig. 6 shows the time required for each actuator to reach the temperature of 60 °C ($t_{60°C}$) under various applied currents from 0.8 A to 1.7 A for Actuator-1 and 0.6 A to 1.3 A for Actuator-2. Heating was faster in Actuator-2 than Actuator-1, because it had smaller free surface for each wire segment embed-

Table 1
Material properties of SMA wire [19].

Martensite Young's modulus (E_M)	Austenite Young's modulus (E_A)	Martensite start temperature (M_s)	Martensite finish temperature (M_f)	Austenite start temperature (A_s)	Austenite finish temperature (A_s)
28 GPa	75 GPa	52 °C	42 °C	68 °C	78 °C

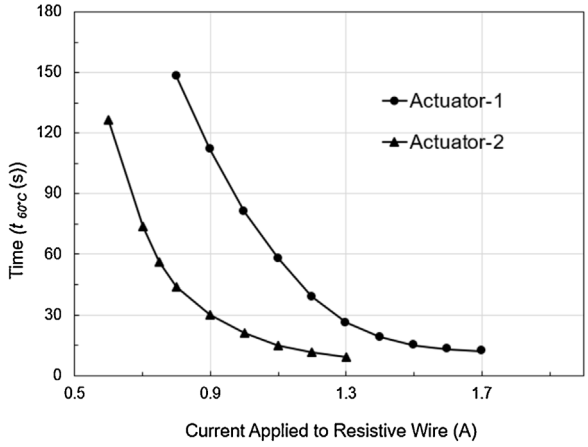

Fig. 6. The time required for the SMP segments of a) Actuator-1, and b) Actuator-2, to reach a temperature of 60 °C under various applied currents. Temperature was measured at Point C on Actuator-1 (Fig. 1a), and at Point E on Actuator-2 (Fig. 1b).

ded within the actuator, hence dissipated heat through convection to the ambient air at a lower rate.

As observed in Fig. 6, the current of 1.1 A and 0.75 A should be applied to the resistive wires embedded into the SMP segments of Actuator-1 and Actuator-2, respectively, to increase the SMP temperature to 60 °C in less than 60 s. For consistency, in all of the remaining experiments these currents were applied to Actuator-1 and Actuator-2 to ensure identical heating times for both actuators.

The change of actuators temperature with time near SMP and SMA (Points C and D in Fig. 1a, and Points E and F in Fig. 1b) was also measured. To this end, the currents of 1.1 A and 0.75 A were applied for 60 s to the resistive wires of Actuator-1 and Actuator-2, respectively.

Fig. 7 shows that the heat generated by resistive wires in the SMP segments also increases the actuator temperature near the SMA wire. This temperature increase is more significant in Actuator-2 owing to the small distance between the resistive and SMA wires in this actuator. It is worth noting, however, that the maximum SMA temperature in both actuators never exceeds the austenite start temperature (A_s = 68 °C; Table 1). Therefore, in none of the actuators applying electric currents to the resistive wires actuates the SMA wires.

A key parameter governing the strength of the fabricated actuators is the bending stiffness. Since the embedded SMA and resistive wires have a very small volume, it is assumed they have a negligible effect on the bending stiffness. Thus the bending stiffness of the actuators in the hinge area is solely determined by the soft and SMP segments from the following equation:

$$E_A I_A = E_{Soft} I_{Soft} + E_{SMP} I_{SMP} \quad (1)$$

where E_A, E_{Soft}, and E_{SMP} show the Young's modulus of the actuator, soft and SMP segments, respectively. I_A, I_{Soft}, and I_{SMP} denote the second moment of area of the actuator, soft and SMP segments, respectively. All parameters in Eq. (1) are constant, except E_{SMP}, which is much higher in glassy state than the rubbery state, as shown in Fig. 3a and b. Since the soft material has a very low glass transition temperature (FLX9960, T_g = 4 °C), it remains in rubbery state over the entire range of operation temperature. Therefore, it is assumed that the Young's modulus of the actuators soft segments is constant.

The change of the actuators bending stiffness during cooling, from T = 60 °C to T = 25 °C, was calculated using Eq. (1), and plotted in Fig. 8. The thickness of the SMP segments of the actuators in the hinge area was assumed to be 2 mm. The Young's modulus of the SMP, VeroClear, for different temperatures was extracted from Fig. 3a. As expected, Fig. 8 confirms that the bending stiffness of the actuator substantially changes with temperature. The bending stiffness of Actuator-1 at high temperature (60 °C) and

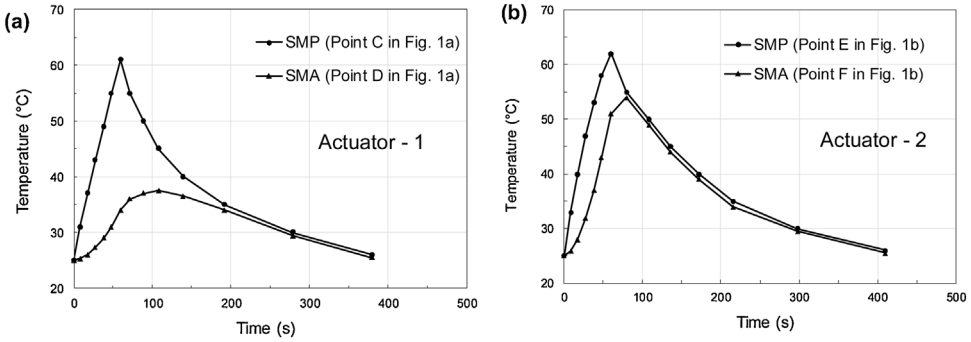

Fig. 7. Variation of the actuators temperature near the SMA and SMP with time. The current of 1.1 A and 0.75 A was applied for 60 s to the resistive wires embedded into Actuator-1 and Actuator-2, respectively. a) Actuator-1 (Fig. 1a). b) Actuator-2 (Fig. 1b).

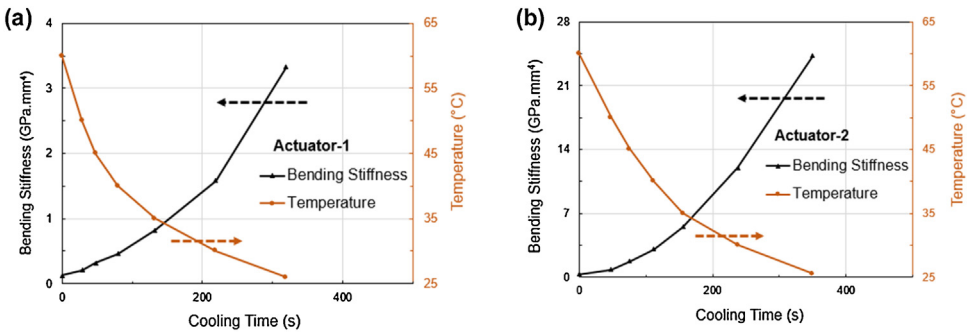

Fig. 8. Variation of the bending stiffness and temperature of the actuators with time during cooling. a) Actuator-1 (Fig. 1a). b) Actuator-2 (Fig. 1b).

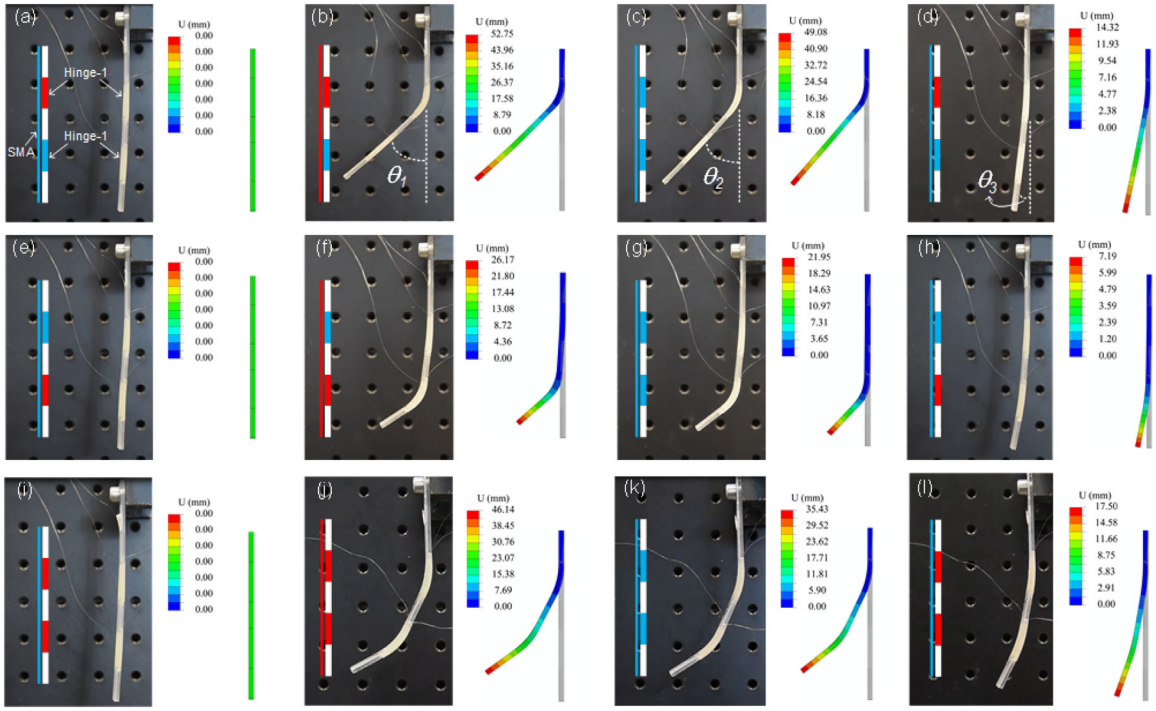

Fig. 9. Experimental and numerical results of the independent and simultaneous actuation of Hinge-1 and Hinge-2 of Actuator-1 (Figs. 1a and 5). Blue and red colors of the hinges in the insets indicate the glassy state at room temperature and rubbery state at high temperature, respectively, realized by Joule heating through resistive wires. Blue and red colors of the SMA inset show the actuated and unactuated state of the SMA wire. The color contours show the actuator displacement in different configurations. a-d) Original and deformed configurations of Hinge-1 (the top hinge) of Actuator-1. e-h) Original and deformed configurations of Hinge-2 (the bottom hinge) of Actuator-1. i-l) Simultaneous actuation of Hing-1 and Hinge-2 of Actuator-1.

low temperature (25 °C) was determined to be 0.13 GPa.mm^4 and 3.32 GPa.mm^4, respectively, indicating 96.2% reduction of bending stiffness at high temperatures. For Actuator-2, the bending stiffness changed from 0.33 GPa.mm^4 at high temperature to 24.3 GPa.mm^4 at room temperature, corresponding to 98.6% change in the stiffness. These results show the great stiffness variability of both actuators, which helps achieve desired performance for the soft robotics applications.

Overall, Fig. 8 shows that Actuator-2 is one order of magnitude stiffer than Actuator-1 at room temperature, and demonstrates a more significant change in stiffness with temperature, simply because it contains a larger volume of the SMP in the hinge areas.

Applying electric current to the resistive wires inserted into each hinge enables independent actuation of each of the actuator hinges. After the SMP segment of the desired hinge becomes soft via Joule heating, the SMA wire is actuated to deform the actuator. Fig. 9 compares the experimental and finite element results of the independent and simultaneous actuation of the hinges of Actuator-1 with the hinge SMP thickness of 2 mm (Fig. 1a).

The experimental actuation steps are as follow. First, the current of 1.1 A was applied to the resistive wire of the desired hinges for 60 s to heat up the SMP to 60 °C (Fig. 9a, e and i). Then, the resistive wire was switched off, and the current of 0.41 A was applied to the SMA, while the desired hinge was still at high temperature rubbery state, as shown in Fig. 9b, f, and j. This caused the actuator to bend from the heated hinge. The SMA wire was maintained in the actuated state for 120 s to give enough time to the SMP to cool down and become glassy. Fig. 9c, g and k show that the actuator was able to retain the deformed shape after the SMA wire was deactivated. However, it slightly bounced back after the SMA current was switched off. Finally, to restore the actuator original shape, the current of 1.1 A was applied again to the respective resistive wire (Fig. 9d, h, and l).

Movie S1 shows the actuator performance during a full cycle of deformation for Actuator-1 with the hinge SMP thickness of 2 mm, while Movie S2 demonstrates the finite element results of deformation cycle for the same actuator. It should be noted that without a shape retention mechanism, the current must be continuously supplied to the SMA wire so that its temperature remains higher than the SMA actuation temperature, and the actuator could remain in the deformed state. Here, the continuous consumption of energy was avoided by utilizing the printed SMP segments for shape retention.

In order to characterize the shape fixity and recovery of the bending actuators, the shape fixing ratio (R_f) was used to determine their ability to retain a temporary shape, and the shape recovery ratio (R_r) to measure its ability to restore its initial straight shape. R_f and R_r were calculated using the following two equations:

$$R_f = \theta_2/\theta_1 \text{ and } R_r = 1 - \theta_3/\theta_2 \quad (2)$$

where θ_1, θ_2 and θ_3 are defined in Fig. 9b and d. In Eq. (2), θ_1 indicates the maximum rotation angle of the actuator before deactivating the SMA wire, θ_2 indicates the rotation angle after deactivating the SMA wire, and θ_3 is the rotation angle after recovery.

The SMP layer in the hinge area of Actuator-1 and Actuator-2 is shown in cross-section A-A in Fig. 1a and cross-section B-B in Fig. 1b, respectively. As seen in Fig. 1, the SMP volume in Actuator-2 is larger than Actuator-1. In a series of experiments, the thickness of the SMP segments in the hinge area was varied for both Actuator-1 and Actuator-2 to study its effect on the rotation angle, bending stiffness, recovery and fixity of Hinge-1. The results were compared with the finite element simulations described in Section 3.

Fig. 10a demonstrates the variation of the bending stiffness of the Actuator-1 and Actuator-2 with the thickness of the SMP

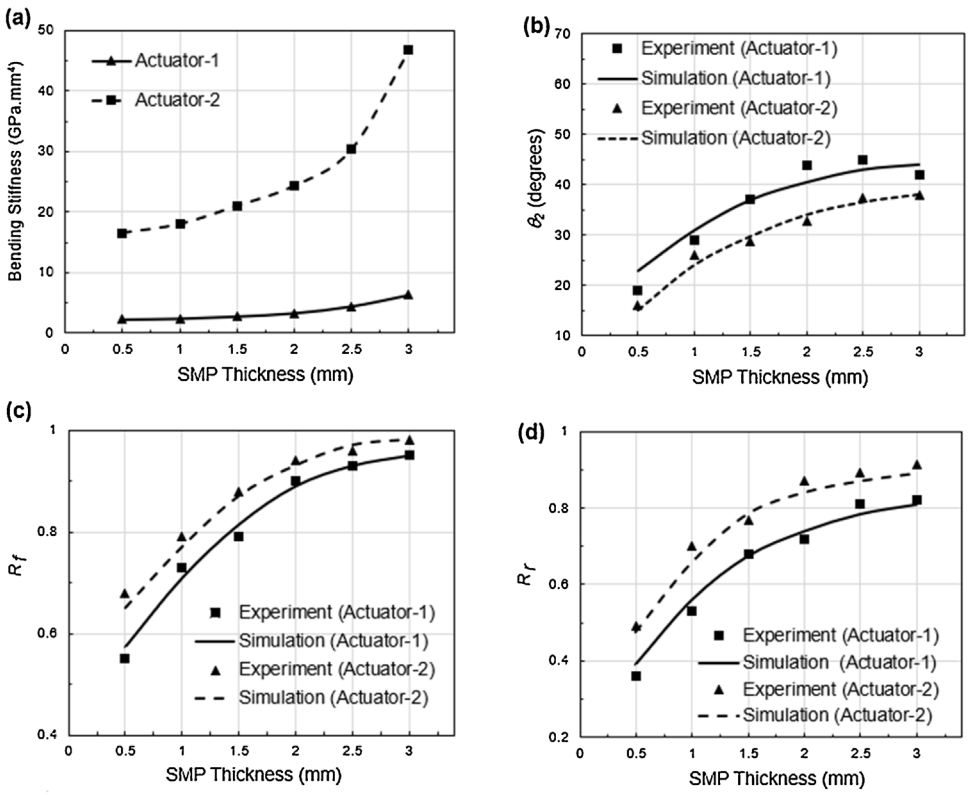

Fig. 10. Effect of the SMP thickness on the a) bending stiffness, b) rotation angle, c) recovery ratio, and d) fixity of Hinge-1 of Actuator-1 and Actuator-2. The SMP thickness in the hinge area was varied from 0.5 mm to 3 mm.

layer in the hinge area at room temperature. With increase of the SMP thickness from 0.5 mm to 3.0 mm, the stiffness of Actuator-1 increases from 2.3 GPa mm^4 to 6.3 GPa mm^4, while the stiffness of Actuator-2 changes from 16.5 GPa mm^4 to 46.8 GPa mm^4. Therefore, multimaterial 3D printing enables stiffness variation not just by printing various designs with complex arrangements of soft elastomer and rigid SMP segments, but also by varying the SMP thickness in a specific design.

Fig. 10b-d show that the finite element model is able to predict the effect of the SMP thickness on the maximum rotation angle (θ_2 in Fig. 9c), shape fixity, and recovery ratio with good accuracy. Fig. 10b shows that the maximum rotation angle for Actuator-1 is always larger than Actuator-2, because Actuator-2 uses a larger amount of the SMP in the hinge area, which increases the stiffness of the hinge in the rubbery state and limits its maximum rotation. On the other hand, this causes the shape fixity and recovery of Actuator-2 to be always larger than Actuator-1 for a specific thickness. In general, the use of more SMP in the hinge area increases its ability to retain the actuated bent shape and recover the original straight shape. These findings show that for each specific application, using multimaterial 3D printing the actuator design can be modified to achieve the desired performance.

To demonstrate the application of the fabricated actuators in soft robotics, a soft fingered gripper was designed and printed based on the Actuator-1 design (Fig. 11a). Fig. 11b features a symmetrical gripper with three identical fingers in a triangular configuration, each having two hinges following the design of Actuator-1. A rigid structure printed from VeroClear was used as a base for the fingers, and a small arc-shaped extrusion printed part at the end of each finger simulated a fingernail. The gripper had both SMA and resistive wires connected in series for simultaneous actuation of all the fingers. A 150 g cylindrical object, as depicted in Fig. 11c, was steadily grasped, effectively lifted, concretely held, and then placed back to the original position within 20 s. To adjust the gripper force handling capabilities based on each specific application, the bending rigidity and deformation could be easily modulated as desired earlier by integrating spatial variation and selective material change as well as individual actuation of the SMA wire for each finger. This enables a soft, adaptive, and stable grasping of 3D objects with increased geometric complexity. For this purpose, the three-dimensional numerical framework established in Section 3 can be exploited as an effective tool to optimize design for specific force handling capability requirements. The numerical method can be supplemented with analytical models available for SMA-elastomer composites to investigate the effect of crucial parameters influencing the actuator performance such as moment-curvature relation and asymmetry in SMA behavior [31–33].

5. Conclusions

This study demonstrated the great capability of multimaterial inkjet 3D printing to manufacture variable stiffness composite actuators capable of shape retention and shape recovery. The stiffness modulation of these SMA-based actuators is realized by changing the temperature of the printed SMP segments via Joule heating. The shape retention capability reduces the energy required to maintain the deformed shape of the actuator. Furthermore, the shape memory behavior of the SMP allows for recovery of the initial undeformed shape without applying any external mechanical load. The hinge design was also modified to control maximum deformation, bending stiffness, and fixity and recovery ratios of the actuators. It was shown that the use of larger amount of SMP in the hinge area increases the fixity and recovery, but limits the maxi-

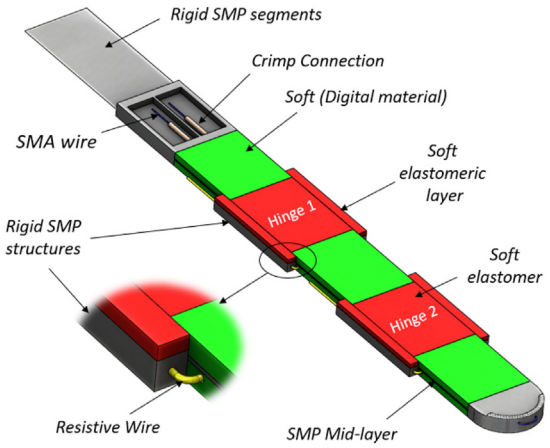

(a)

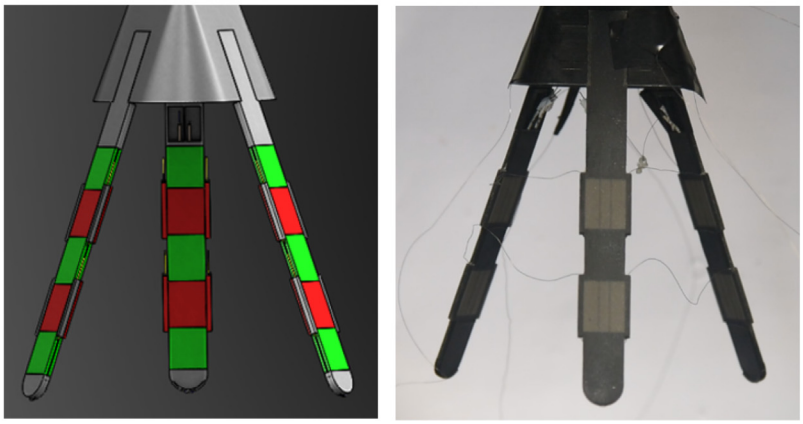

(b)

(c)

Fig. 11. a) Detailed view of the robotic gripper finger design. b) Fabricated gripper based on the the Actuator-1 design. c) Grasping action of the gripper.

mum deformation due to increased bending stiffness in the hinge area.

The fabrication of shape reversible composite actuators by multimaterial 3D printing has many advantages over conventional molding and casting methods. Multimaterial inkjet 3D printing enables arrangement of distinctive soft and rigid SMP polymers with high precision and controllability. Moreover, morphological and geometric complexity of the 3D printed parts does not increase time or cost of fabrication. It provides designers with greater freedom to print intricate features necessary to address various structural requirements. Although the printing method used here is limited to a few commercially available materials, but further development of 3D printable materials in future will increase the possibility of printing even more complex active structures.

Author statement

We declare there are no financial and personal relationships with other people or organizations that could inappropriately influence (bias) this work.

Declaration of Competing Interest

We declare there are no financial and personal relationships with other people or organizations that could inappropriately influence (bias) this work.

Acknowledgement

The authors acknowledge support from SUTD Digital Manufacturing and Design Centre (DManD) funded by Singapore National Research Foundation (NRF). Q. G. acknowledges the support from the Agency for Science, Technology and Research (A*STAR) Public Sector Funding (PSF) (Project number 1521200086), the U.S. Office of Naval Research Global (ONRG), and the SUTD Start-up Research Grant.

References

[1] M. Ashir, A. Nocke, C. Theiss, C. Cherif, Development of adaptive hinged fiber reinforced plastics based on shape memory alloys, Compos. Struct. 170 (2017) 243–249.
[2] B. Holschuh, E. Obropta, D. Newman, Low spring index NiTi coil actuators for use in active compression garments, IEEE/ASME Trans. Mechatron. 20 (3) (2015) 1264–1277.
[3] S. Barbarino, E.S. Flores, R.M. Ajaj, I. Dayyani, M.I. Friswell, A review on shape memory alloys with applications to morphing aircraft, Smart Mater. Struct. 23 (6) (2014) 063001.
[4] U. Icardi, L. Ferrero, Preliminary study of an adaptive wing with shape memory alloy torsion actuators, Mater. Des. 30 (10) (2009) 4200–4210.
[5] Z. Wang, G. Hang, Y. Wang, J. Li, W. Du, Embedded SMA wire actuated biomimetic fin: a module for biomimetic underwater propulsion, Smart Mater. Struct. 17 (2) (2008), 025039.
[6] H.A. Bruck, C.L. Moore, T.L. Valentine, Repeatable bending actuation in polyurethanes using opposing embedded one-way shape memory alloy wires exhibiting large deformation recovery, Smart Mater. Struct. 11 (4) (2002) 509.
[7] D.C. Lagoudas, I.G. Tadjbakhsh, Active flexible rods with embedded SMA fibers, Smart Mater. Struct. 1 (2) (1992) 162.
[8] H. Rodrigue, W. Wang, M.-W. Han, T.J. Kim, S.-H. Ahn, An overview of shape memory alloy-coupled actuators and robots, Soft Robot. 4 (1) (2017) 3–15.
[9] H. Rodrigue, W. Wang, D.-R. Kim, S.-H. Ahn, Curved shape memory alloy-based Soft actuators and application to Soft gripper, Compos. Struct. (2017).
[10] W. Wang, H. Rodrigue, H.-I. Kim, M.-W. Han, S.-H. Ahn, Soft composite hinge actuator and application to compliant robotic gripper, Compos. Part B Eng. 98 (2016) 397–405.
[11] W. Wang, H. Rodrigue, S.-H. Ahn, Smart soft composite actuator with shape retention capability using embedded fusible alloy structures, Compos. Part B Eng. 78 (2015) 507–514.
[12] S.-H. Song, J.-Y. Lee, H. Rodrigue, I.-S. Choi, Y.J. Kang, S.-H. Ahn, 35 Hz shape memory alloy actuator with bending-twisting mode, Sci. Rep. 6 (2016).
[13] J.J. Song, Q. Chen, H.E. Naguib, Constitutive modeling and experimental validation of the thermo-mechanical response of a shape memory composite containing shape memory alloy fibers and shape memory polymer matrix, J. Intell. Mater. Syst. Struct. 27 (5) (2016) 625–641.
[14] H. Rodrigue, W. Wang, M.-W. Han, Y.-J. Quan, S.-H. Ahn, Comparison of mold designs for SMA-based twisting soft actuator, Sens. Actuators A Phys. 237 (2016) 96–106.
[15] C. Lelieveld, K. Jansen, P. Teuffel, Mechanical characterization of a shape morphing smart composite with embedded shape memory alloys in a shape memory polymer matrix, J. Intell. Mater. Syst. Struct. 27 (15) (2016) 2038–2048.
[16] P. Ghosh, A. Rao, A.R. Srinivasa, Design of multi-state and smart-bias components using shape memory alloy and shape memory polymer composites, Mater. Des. 44 (2013) 164–171.
[17] M. Taya, Y. Liang, O.C. Namli, H. Tamagawa, T. Howie, Design of two-way reversible bending actuator based on a shape memory alloy/shape memory polymer composite, Smart Mater. Struct. 22 (10) (2013), 105003.
[18] B.E. Schubert, D. Floreano, Variable stiffness material based on rigid low-melting-point-alloy microstructures embedded in soft poly (dimethylsiloxane)(PDMS), RSC Adv. 3 (46) (2013) 24671–24679.
[19] W. Wang, S.-H. Ahn, Shape memory alloy-based Soft gripper with variable stiffness for compliant and effective grasping, Soft Robot. 4 (4) (2017) 379–389.
[20] M.A. McEvoy, N. Correll, Thermoplastic variable stiffness composites with embedded, networked sensing, actuation, and control, J. Compos. Mater. 49 (15) (2015) 1799–1808.
[21] H. Tobushi, S. Hayashi, Y. Sugimoto, Two-way bending properties of shape memory composite with SMA and SMP, Materials 2 (3) (2009) 1180–1192.
[22] Y. Mao, Z. Ding, C. Yuan, S. Ai, M. Isakov, J. Wu, et al., 3D printed reversible shape changing components with stimuli responsive materials, Sci. Rep. 6 (2016) 24761.
[23] Y. Mao, K. Yu, M.S. Isakov, J. Wu, M.L. Dunn, H.J. Qi, Sequential self-folding structures by 3D printed digital shape memory polymers, Sci. Rep. 5 (2015) 13616.
[24] Q. Ge, C.K. Dunn, H.J. Qi, M.L. Dunn, Active origami by 4D printing, Smart Mater. Struct. 23 (9) (2014) 094007.
[25] Q. Ge, H.J. Qi, M.L. Dunn, Active materials by four-dimension printing, Appl. Phys. Lett. 103 (13) (2013) 131901.
[26] S. Akbari, A.H. Sakhaei, S. Panjwani, K. Kowsari, A. Serjouei, Q. Ge, Multimaterial 3D printed soft actuators powered by shape memory alloy wires, Sens. Actuators A Phys. 290 (May) (2019) 177–189, 1.
[27] A.H. Sakhaei, P. Thamburaja, A finite-deformation-based constitutive model for high-temperature shape-memory alloys, Mech. Mater. 109 (2017) 114–134.
[28] D.C. Lagoudas, Z. Bo, M.A. Qidwai, A unified thermodynamic constitutive model for SMA and finite element analysis of active metal matrix composites, Mech. Compos. Mater. Struct. 3 (2) (1996) 153–179.
[29] K.K. Westbrook, P.H. Kao, F. Castro, Y. Ding, H.J. Qi, A 3D finite deformation constitutive model for amorphous shape memory polymers: a multi-branch modeling approach for nonequilibrium relaxation processes, Mech. Mater. 43 (12) (2011) 853–869.
[30] K. Yu, Q. Ge, H.J. Qi, Reduced time as a unified parameter determining fixity and free recovery of shape memory polymers, Nat. Commun. 5 (2014) 3066.
[31] G. Wang, M. Shahinpoor, Design, prototyping and computer simulations of a novel large bending actuator made with a shape memory alloy contractile wire, Smart Mater. Struct. 6 (2) (1997) 214.
[32] N.V. Viet, W. Zaki, R. Umer, Analytical model of functionally graded material/shape memory alloy composite cantilever beam under bending, Compos. Struct. 203 (2018) 764–776.
[33] N.V. Viet, W. Zaki, Bending model for a laminated composite cantilever beam with multiple embedded shape memory alloy layers presenting tensile-compressive asymmetry, Compos. Struct. 229 (2019) 111410.

Biographies

Saeed Akbari is a researcher at RISE Research Institutes of Sweden. He received his PhD from University of Toronto, Canada, at 2017. His research interests include additive manufacturing, active materials, polymer composites & nanocomposites, electronic packaging and board level reliability tests.

Amir Hosein Sakhaei is an Assistant Professor at the University of Kent, UK. He obtained his PhD from National University of Singapore at 2014. His research focuses on theoretical and computational mechanics of advanced materials, continuum mechanics, finite element simulations, and advanced manufacturing.

Sahil Panjwani is a Research Assistant at Singapore University of Technology and Design (SUTD). His research interests include robotics, Computer-Aided-Engineering (CAE), and 3D printing. He received his Bachelor of Technology from Manipal University Jaipur, India, at 2017.

Kavin Kowsari has worked as postdoctoral research fellow at Massachusetts Institute of Technology as well as Singapore University of Technology and Design (SUTD). He received his PhD from University of Toronto, Canada, at 2017. His research areas are additive manufacturing, 3D/4D printing, biofabrication, soft robotics, and computational fluid dynamics.

Qi Ge is an associate professor at Southern University of Science & Technology, China. He previously worked as an assistant professor at Singapore University of Technology and Design (SUTD). He received his PhD from University of Colorado Boulder at 2012. He is a well-known researcher in the areas of 4D printing, shape memory polymers, and functional printable materials.